



## PAPER

## Coherent control for qubit state readout

## OPEN ACCESS

RECEIVED  
5 March 2020REVISED  
11 May 2020ACCEPTED FOR PUBLICATION  
4 June 2020PUBLISHED  
23 July 2020Conrad Roman<sup>1</sup>, Anthony Ransford, Michael Ip and Wesley C Campbell

University of California Los Angeles, United States of America

<sup>1</sup> Author to whom any correspondence should be addressed.E-mail: [conradhr@physics.ucla.edu](mailto:conradhr@physics.ucla.edu)

Keywords: coherent control, quantum information, trapped ions

Original content from  
this work may be used  
under the terms of the  
[Creative Commons  
Attribution 4.0 licence](#).

Any further distribution  
of this work must  
maintain attribution to  
the author(s) and the  
title of the work, journal  
citation and DOI.



### Abstract

Short pulses from mode-locked lasers can produce background-free atomic fluorescence by allowing temporal separation of the prompt incidental scatter from the subsequent atomic emission. We use this to improve our quantum state detection of optical-frequency and electron-shelved trapped ion qubits by more than two orders of magnitude. For direct detection of qubits defined on atomic hyperfine structure, however, the large bandwidth of short pulses is greater than the hyperfine splitting, and repeated excitation is not qubit state selective. Here, we show that the state resolution needed for projective quantum measurement of hyperfine qubits can be recovered by applying techniques from coherent control to the orbiting valence electron of the queried ion. We demonstrate electron wavepacket interference to allow readout of the original qubit state using broadband pulses, even in the presence of large amounts of background laser scatter.

An essential capability of a quantum information processor is the ability to read out the result of the computation [1]. Since these devices are susceptible to information corruption, it is also likely some form of quantum error correction will be required to perform even moderately lengthy computations, and repeated qubit state detections will be needed during operation [2]. The primary metrics for evaluating the quality of qubit measurement for these tasks, therefore, are the fidelity [3] and speed [4], both of which frequently compare poorly to gate operations.

State readout in trapped ion processors is typically performed by illuminating ions with a continuous-wave (cw) laser resonant with a cycling transition that contains one qubit state (the so-called ‘bright state’) and not the other (the ‘dark state’) [5–7]. When an ion qubit is in the bright state, laser-induced fluorescence (LIF) photons are collected by high-NA imaging optics, spatially filtered from the incidental laser scatter, and counted using a photomultiplier tube (PMT). A dark state ion qubit, on the other hand, will not fluoresce and with ideal spatial filtering of the excitation light, no photons will be counted. For atomic hyperfine qubits, the state interrogation time is typically limited by off-resonant absorption of photons that mix the qubit basis states [8]. Higher efficiency collection of the fluorescence typically improves both the fidelity and speed of the readout [4, 9–11].

As trapped ion quantum processors continue to miniaturize [12–14] and integrate photonic elements onto the trap chip [15, 16], the ions are held increasingly close to surfaces that scatter excitation light toward the detector, and background scatter, as opposed to collection efficiency, can become the limiting factor in readout speed and fidelity [17]. In particular, scalable systems incorporating chip-integrated non-imaging single-photon detectors [18, 19] can achieve very high detection efficiency (particularly as the ion is moved closer to the detector), but must rely on other mechanisms for rejecting background scatter [20, 21].

In this work, we report the use of a mode-locked laser to achieve qubit state detection that is nearly background free by counting photons only in the dark time between the excitation pulses. We first apply this method to detection of electron-shelved [22] hyperfine qubits, where the resolution required for state selectivity ( $\approx 170$  THz) is much larger than the bandwidth of the pulse ( $\approx 50$  GHz). Temporal rejection of background scatter eliminates it as a constraint [23] and allows us to achieve a factor of 100 improvement in the signal to background ratio for single-shot detection with an average fidelity of  $\mathcal{F} = 0.9993^{+0.0003}_{-0.0006}$  in

the presence of  $\approx 45\,000$  background counts per second. For un-shelved hyperfine qubits, however, the pulse bandwidth far exceeds the frequency resolution required for state selectivity ( $\approx 2$  GHz). Here, we bring together techniques from quantum information science and coherent control, and use Ramsey spectroscopy to gain a sub-femtosecond view of the complex motion of the valence electron orbiting this single atom between excitation pulses. This unique, time-domain picture of the inner workings of a quantum bit allows us to discern and control the microscopic dynamics of the atom's electron to demonstrate direct detection of the qubit state by suppressing unwanted excitations through destructive interference of electron wavepackets. This demonstration suggests that further application of coherent control techniques to quantum information science may provide solutions to some of the challenges facing the creation of large-scale, programmable quantum processors.

The qubit in this work is hosted by a single  $^{171}\text{Yb}^+$  ion confined in a radio frequency Paul trap with oblate spheroidal symmetry [24]. The hyperfine clock-state qubit is defined in the ground  $^2\text{S}_{1/2}$  state by the levels  $|0\rangle \equiv |F''=0, m_{F''}=0\rangle$  and  $|1\rangle \equiv |F''=1, m_{F''}=0\rangle$  [25], shown in figure 2(a). For each experiment, after cw Doppler cooling of the ion's motion, qubit state preparation is performed by optical pumping to the  $|0\rangle$  state via resonant, cw excitation to the excited  $|^2\text{P}_{1/2}^0; F=1\rangle$  manifold. Single-qubit gates for population transfer between qubit states are provided by resonant microwaves delivered via a microwave antenna.

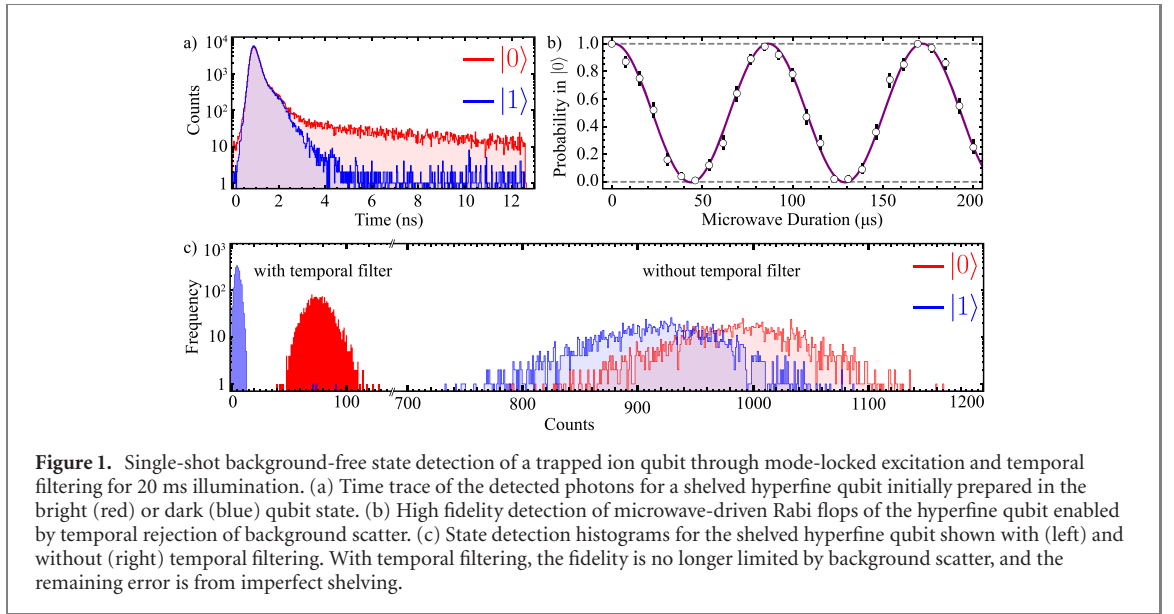
In the typical, cw laser driven  $I=\frac{1}{2}$  qubit state readout scheme [8],  $|1\rangle$  acts as the bright state; a single-frequency cw laser resonant with  $|^2\text{S}_{1/2}; F''=1\rangle \rightarrow |^2\text{P}_{1/2}^0; F=0\rangle$  is applied and excited atoms spontaneously decay back to  $|^2\text{S}_{1/2}; F''=1\rangle$  with high probability [25]. This cycle is driven until the probability that off-resonant excitation mixes the qubit states limits the fidelity. In contrast, for electron-shelved detection [22],  $|0\rangle$  plays the role of bright state; population in  $|1\rangle$  is transferred ('shelved') to a metastable state and photon collection during subsequent cw Doppler cooling is used to discern whether the ion was shelved. For shelving of  $^{171}\text{Yb}^+$  hyperfine qubits [26], we apply a laser at 411 nm to transfer population from  $|1\rangle$  to the effectively stable  $^2\text{F}_{7/2}^0$  state via the  $^2\text{D}_{5/2}$  state. Subsequent illumination at 369.5 nm and 935.2 nm reveals essentially unlimited LIF for an ion found in  $|0\rangle$ , whereas an ion initially in  $|1\rangle$  has been shelved and is dark.

For the pulsed qubit state detection in this work, excitation of the bright state population to  $^2\text{P}_{1/2}^0$  is driven by a frequency doubled mode-locked (ML) laser generating near-transform-limited  $\approx 10$  ps pulses at 369.5 nm with a repetition rate of  $f_r = 79.5$  MHz. Because the laser-excited  $^2\text{P}_{1/2}^0$  state has a lifetime of  $\tau = 8.12$  ns [27], an atom excited by a pulse from the ML laser will emit a photon with high (78%) probability before the next pulse arrives. Nonetheless, multi-pulse coherence can still lead to strong comb tooth effects [28], and the positions of the laser's optical frequency comb teeth in this work are held far from any resonances by an intra-cavity piezo-mounted mirror. Pulse energies at the ion are typically  $\approx 0.25$  pJ, corresponding to a rotation of the atomic  $^2\text{S}_{1/2} \leftrightarrow ^2\text{P}_{1/2}^0$  Bloch vector of  $\theta \approx 0.05\pi$ . Ion fluorescence at 369.5 nm is collected by an objective lens and registered by a PMT through a 369 nm bandpass filter (transmissivity  $\approx 90\%$ ). The photon counting PMT has a quantum efficiency of 27% at 369 nm, and its output is monitored by either an FPGA-based photon time tagger ( $\approx 10$  ns resolution [29]) or a fast, time correlated single photon counter (TCSPC,  $\approx 25$  ps resolution<sup>2</sup>). The imaging system has an effective numerical aperture of 0.19, resulting in an end-to-end photon detection efficiency of  $\approx 0.16\%$ .

For shelved and optical-frequency qubits, the population in  $^2\text{F}_{7/2}^0$  is well separated from the ground and excited states (by  $> 100$  THz) and sits far outside the spectral bandwidth of the excitation pulse. Figure 1(a) shows a time trace of the collected photons from many repeated excitations of a single ion initially prepared in the dark ( $|1\rangle$ , blue trace) and bright ( $|0\rangle$ , red trace) hyperfine qubit states, after attempted shelving. The prompt peak near  $t = 1$  ns is caused by incidental laser scatter, and is extinguished below the level of dark counts ( $40\text{ s}^{-1}$ ) in about 4 ns. The observed pulse width of greater than 100 ps is due to the transit time spread of photo-electrons in the PMT. The window from  $\approx 3$ –12.5 ns, in which an initially excited ion will emit a photon with roughly 50% probability, allows fluorescence detection that is essentially free of corruption by background scatter.

By separately recording the number of collected photons for an ion initially prepared in dark state and the bright state for many repetitions, histograms of the two results are constructed (figure 1(c)). Well-separated histograms are required for single-shot state detection, where a threshold is typically chosen between the two distributions to discriminate the two states. However, the total collected light, shown on the right side of figure 1(c), shows substantial overlap of the two histograms and poor state discrimination

<sup>2</sup> Picoquant timeharp 260P



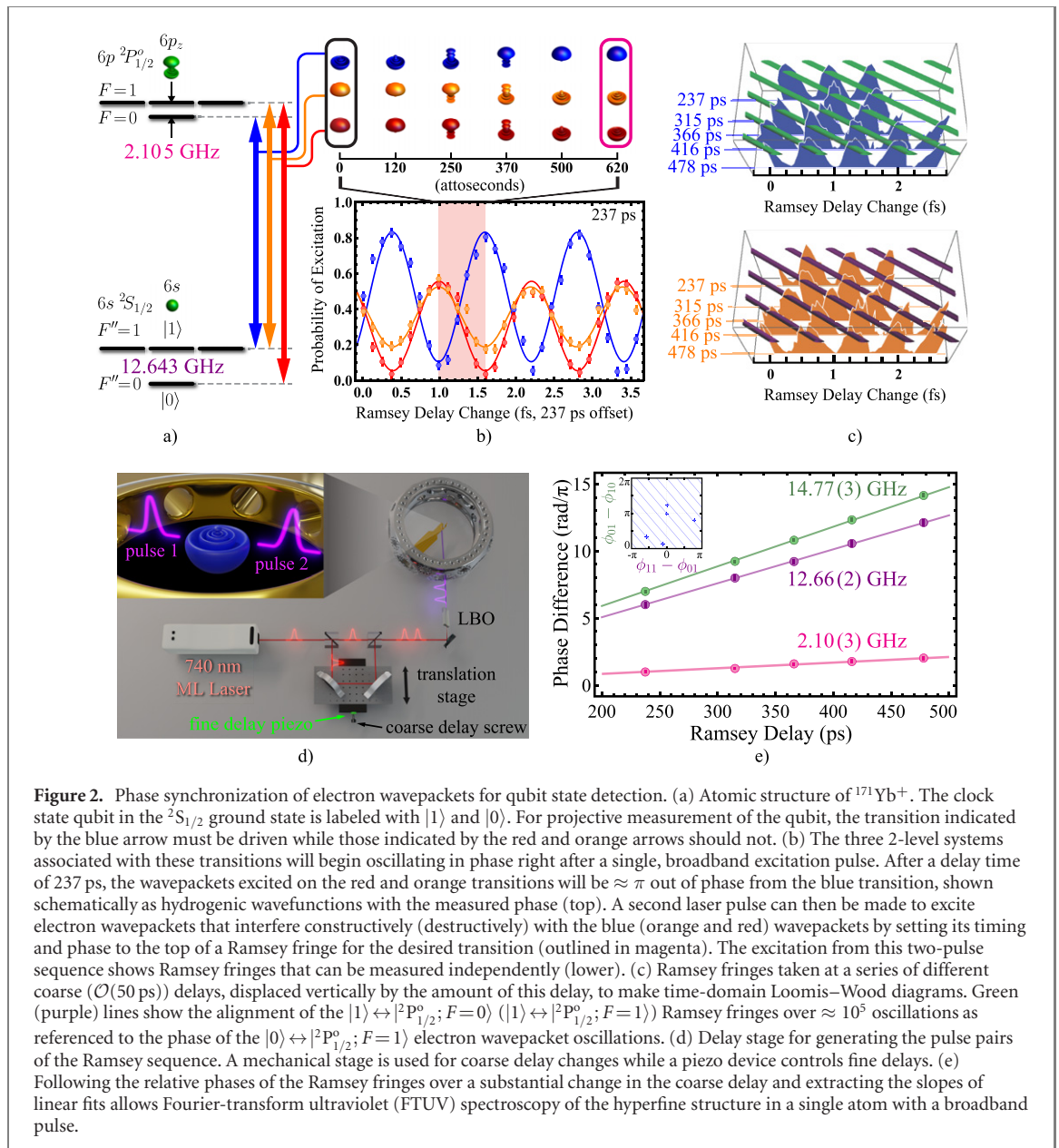
due to incidental scatter from the excitation laser, yielding an average single-shot detection fidelity of  $\mathcal{F} = 0.76 \pm 0.01$  using a threshold.

In contrast, by repeating the same experiment while rejecting counts outside the background-free window, shown by the solid histograms on the left side of figure 1(c), essentially all of the substantial technical scatter caused by the mode-locked laser can be rejected. This technique achieves an average single-shot detection fidelity of  $\mathcal{F} = 0.9993^{+0.0003}_{-0.0006}$ , and can be used, for instance, to observe high-contrast Rabi flopping of the qubit (figure 1(b)). As a result, despite the high amount of scatter introduced by using a mode-locked laser for qubit state detection, temporal rejection of background counts effectively eliminates the background scatter as a concern for detection fidelity, boosting performance to a level comparable to cw driven detection of the shelved hyperfine qubit [26]. The remaining errors (the three blue counts in the solid red histogram on the left side of figure 1(c)) are consistent with the bright state histogram and are therefore likely due to incomplete shelving, not poor manifold discrimination. Further improvements in shelving [26] can be used to reduce this infidelity.

To quantify the improvement temporal rejection provides, we consider the signal to noise ratio for qubit state detection,  $\text{SNR} \equiv (\lambda_b - \lambda_d)/\lambda_d$ , where  $\lambda_{b/d}$  is the mean number of detected photons when detecting the bright/dark state. This definition is justified in the case of shelved hyperfine qubits, where the only contributions to noise ( $\lambda_d$ ) are technical. Implementing temporal rejection shows an increase of the SNR from 0.08 to 12.4, a  $\approx 150\times$  increase.

Given the improvement that this technique can provide for scatter-dominated environments, it is well suited for chip-based systems with integrated detectors, where high solid angle can be achieved, but scatter cannot be well filtered spatially. In particular, integrated superconducting nanowire single photon detectors, which feature high efficiency at relevant wavelengths, low dark counts, high maximum count rates, and fast timing resolution, are being integrated into next-generation ion systems [17, 19, 30]. With an estimated fractional solid angle coverage of 5% (taken from the middle of the predicted 3%–8% range for future integrated SNSPDs [19]) and a system detection efficiency of 60%, an optical-frequency qubit (or pre-shelved hyperfine qubit) in the bright state will be able to produce an average of 10 detector counts in  $\approx 5 \mu\text{s}$ . Even if complete temporal filtering of the incidental scatter requires discarding half of these LIF counts, the achievable fidelity is  $> 99\%$  in only  $5 \mu\text{s}$ .

For (un-shelved) hyperfine qubits, which may offer an improvement in aggregate detection speed compared to schemes that require shelving and deshelling steps, the pulse bandwidth ( $\approx 50 \text{ GHz}$ ) encapsulates the entire hyperfine substructure of the cycling transition (which has splittings from 2.105 GHz to 14.748 GHz, see figure 2(a)). Excitation by a single pulse (followed by spontaneous emission) will therefore not only occur for both qubit states, but will also not preserve the total angular momentum  $F''$  of the initial state. For state discrimination, due to finite collection efficiency, the bright state should ideally spontaneously emit many photons on average, while the dark state should not. As shown in figure 2(a), this means the  $|^2S_{1/2}; F''=1\rangle \rightarrow |^2P_{1/2}^0; F=0\rangle$  transition (blue arrow), which will preserve  $F''$ , should be driven while excitations on the other two allowed pathways ( $|^2S_{1/2}; F''=1\rangle \rightarrow |^2P_{1/2}^0; F=1\rangle$  and  $|^2S_{1/2}; F''=0\rangle \rightarrow |^2P_{1/2}^0; F=1\rangle$ , indicated by the orange and red arrows) should be strongly suppressed. To



employ the temporal background rejection technique demonstrated above for direct hyperfine qubit detection therefore requires a means to drive hyperfine-selective optical cycling with the broadband laser.

The route to achieving state selectivity can be found by examining the time dynamics of each excitation, which can be probed through Ramsey (i.e. coherent pump–probe) spectroscopy. To implement a Ramsey experiment, a single pulse from the ML laser is split into two pulses by an imbalanced Mach–Zehnder interferometer (figure 2(d)). The delay of the second pulse with respect to the first is controlled with sub-fs precision by a piezo actuator.

Figure 2(b) (lower) shows three sets of Ramsey fringes obtained from the same ion that allow us to see, with sub-femtosecond resolution, the harmonic motion of the electron wavepacket associated with each of the three, approximately-isolated, two-level systems (TLSs) excited by the first pulse. This simplified 3-TLS model can be used to discern the essential features of the complex dynamics of this multi-level quantum system to engineer a strategy to regain state selectivity. On a microscopic level, the first pulse (or Ramsey zone) excites an electron wavepacket that oscillates at 811 THz in the delay between pulses, illustrated schematically as  $n = 6$  hydrogenic orbital superpositions in figure 2(b) (upper). While the wavepackets corresponding to each of the three TLSs will initially oscillate in phase with one another, the  $\mathcal{O}(10)$  ppm difference between their oscillation frequencies will cause them to slip in relative phase as the delay increases. Figure 2(b) shows the oscillations of each wavepacket after  $\approx 237$  ps of Ramsey delay, at which point the two undesired excitations (shown in orange and red) are approximately  $\pi$  out of phase with the

desired transition (blue). Sinusoidal fits of these data (solid curves) give relative phase differences of  $\Delta\phi_{\text{orange,blue}} = (0.99 \pm 0.04)\pi$  and  $\Delta\phi_{\text{red,blue}} = (0.98 \pm 0.04)\pi$ .

The sub-fs time dynamics of each TLS is probed by performing a series of state preparation and interrogation experiments, each specially tailored to be sensitive to a particular TLS. We confine the duration of pulsed interrogation to the regime where approximately 1 photon is emitted since the emission will tend to mix the qubit states.

CW and microwave preparation of the desired ground state (either  $|0\rangle$  or  $|1\rangle$ ) is followed by a short ( $\approx 4 \mu\text{s}$ ) train of low pulse area ( $\theta \ll \pi/2$ ) Ramsey pairs with the two pulses in each pair separated by the fixed delay of the Mach–Zehnder interferometer. Standard cw state detection is then performed to reveal any population residing in the  $|^2S_{1/2}; F'' = 1\rangle$  manifold. This sequence is repeated as the interferometer phase is scanned to produce the individual Ramsey fringes. Depending on which TLS is being probed, an additional microwave  $\pi$ -pulse may be used before state readout to reorganize population in the ground state. For all fringes, the mode locked laser is  $\pi$ -polarized.

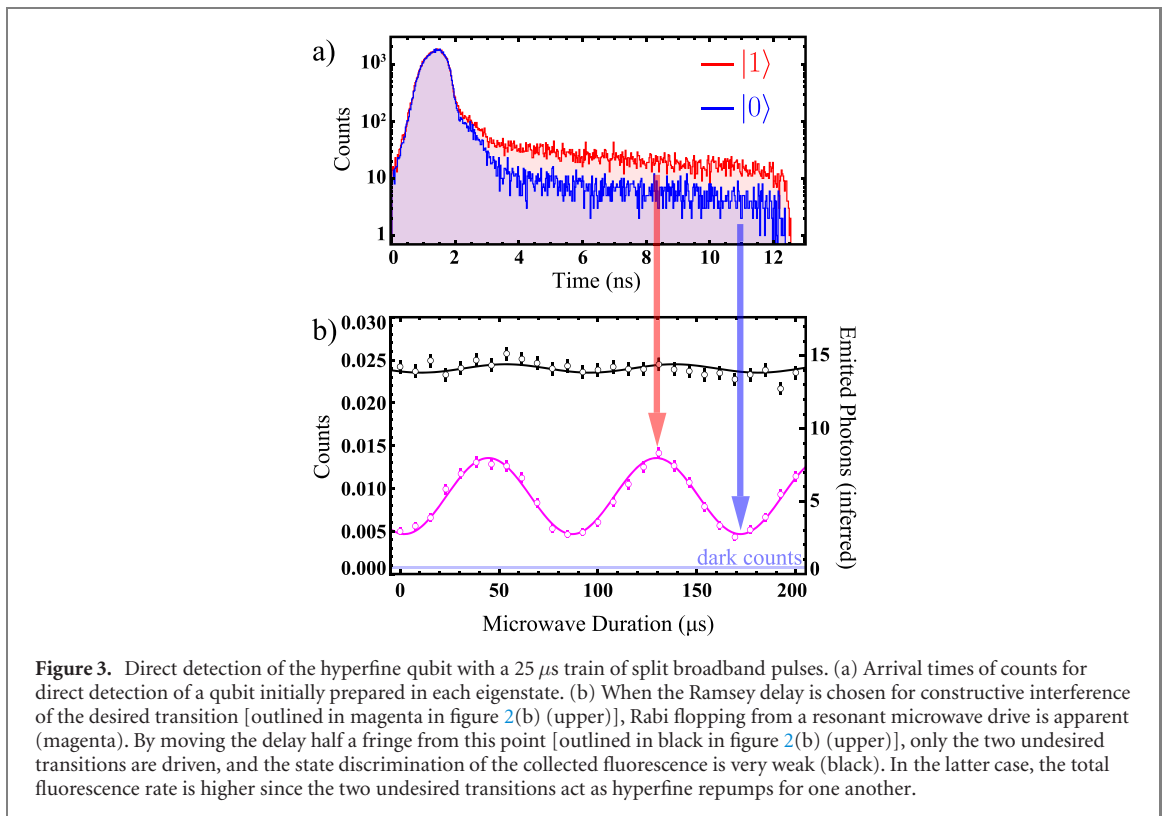
The three fringe acquisition schemes are outlined below, each of which will ideally on average leave the electron in the  $|^2S_{1/2}; F'' = 1\rangle$  bright manifold 2/3 of the time at the top of a fringe (that is, when the full Ramsey sequence leaves the electron in the excited state and it subsequently decays by spontaneous emission), while ideal execution at the bottom of a fringe will leave the population in the  $|^2S_{1/2}; F'' = 0\rangle$  dark state. These values are then used to convert measured populations to excitation probability.

- $|0\rangle \rightarrow |^2P_{1/2}^0; F=1\rangle$  (red in figure 2). The only allowed transition is to the  $|^2P_{1/2}^0; F=1, m_F=0\rangle$  state. Spontaneous emission from this state will on average distribute 1/3 of the population to the original state, and 2/3 to the  $|^2S_{1/2}; F'' = 1\rangle$  manifold.
- $|^2S_{1/2}; F'' = 1\rangle \rightarrow |^2P_{1/2}^0; F=1\rangle$  (blue in figure 2). The  $|^2S_{1/2}; F'' = 1, m_F'' = -1\rangle$  state is prepared initially. The mode locked laser can excite the electron to the  $|^2P_{1/2}^0; F=1, m_F = -1\rangle$  state, after which the population is evenly distributed amongst the  $|^2S_{1/2}; F'' = 1, m_F'' = -1\rangle$ ,  $|1\rangle$ , and  $|0\rangle$  states. Before state readout, a microwave  $\pi$ -pulse is applied between the  $|0\rangle$  and  $|^2S_{1/2}; F'' = 1, m_F'' = -1\rangle$  states.
- $|1\rangle \rightarrow |^2P_{1/2}^0; F=0\rangle$  (orange in figure 2).  $|1\rangle$  is prepared initially, and the only allowed transition is the one of interest. Successful excitation and subsequent spontaneous emission will leave the electron population evenly distributed amongst the  $|^2S_{1/2}; F'' = 1\rangle$  states. Before state readout, a microwave  $\pi$ -pulse is applied between the  $|1\rangle$  and  $|0\rangle$  states.

Ramsey fringes taken at a series of different coarse (tens of picoseconds) delays can be coherently combined only if the number of full ( $2\pi$ ) phase windings between them can be determined. While this is challenging for the optical frequencies here, by choosing one of the three fringe sets to act as a clock reference, phase *differences* between sets will oscillate slower as a function of delay. Figure 2(c) shows the blue (upper) and orange (lower) fringes, translated to set the peak of the red fringe at  $t = 0$ , displayed displaced vertically by their coarse delay in the manner of a Loomis–Wood diagram [31] (see, e.g., [32] for a modern example of the Loomis–Wood technique of molecular spectroscopy). This diagrammatic approach allows patterns in the peaks to be discerned, which are shown as diagonal stripes in figure 2(c). The slope of these lines allow us to follow the phases of the fringes over a range of coarse delays, which amounts to performing Fourier-transform ultraviolet (FTUV) spectroscopy of the qubit atom. Figure 2(e) shows the results of the FTUV spectroscopy, which accurately reproduce the known atomic structure essentially to the level of the natural linewidth ( $1/\tau = 2\pi \times 19.6 \text{ MHz}$ ), roughly 3 orders of magnitude narrower than the pulse bandwidth, and  $50\times$  narrower than the Fourier width of the 500 ps measurement window [33].

By timing the second Ramsey pulse to be centered at the top of the fringe for the desired transition (outlined in magenta at the top of figure 2(b)), constructive interference of the transition amplitude driven by the second pulse with the coherent superposition from the first will drive the desired transition, while the amplitudes of the wavepackets for the two undesired transitions will destructively interfere with the previously excited wavepackets, and all of the population will be returned to the ground state. In the limit of small pulse area, the ratio of the scattering rate of the desired transitions to the two undesired rates is predicted to be  $\kappa \equiv \frac{\Gamma_d}{\sum_u \Gamma_u} \approx \frac{4\Delta}{\gamma} - \frac{1}{2}$ , where  $\gamma$  is the natural linewidth and  $1/2\Delta$  is the delay time between the two pulses. For  $^{171}\text{Yb}^+$ , we calculate  $\kappa \approx 68$  photons can theoretically be spontaneously emitted on average before mixing the qubit.

To evaluate the validity of the 3-TLS model and verify that the temporally-filtered LIF from this two-pulse excitation can be used to perform a direct, projective measurement of the qubit state, a microwave rotation of the qubit is again inserted between state preparation and (now double-pulsed) state detection, shown in figure 3(b). A detection window of  $25 \mu\text{s}$  of illumination by pulse pairs arriving at  $f_r$  is chosen to minimize the probability of state mixing, for which the measured time constant is  $69 \mu\text{s}$ . State mixing as a function of mode-locked pulse pair interrogation time is measured via repeated cw state



preparation and measurement of the qubit states with pulsed interrogation of variable length inserted in the sequence before state readout. Detection of Rabi flopping of the qubit by the microwaves, shown in figure 3(b), shows a fringe visibility of  $V = 0.49 \pm 0.02$  when the phase of the interferometer delay is at the top of the desired fringe (magenta, also outlined in magenta at the top of figure 2(b)), while essentially no state discrimination is evident ( $V = 0.020 \pm 0.009$ ) at the bottom of the same fringe [black, outlined accordingly in figure 2(b)]. The photon arrival times in the desired phase configuration, shown in figure 3(a), show a clear distinction between the two qubit states, though the dark state is not as dark as was the case for the shelved qubit [compare to figure 1(a)]. By taking our total detection efficiency into account, we estimate that the state dependence of the total number of emitted photons [ $\approx 5$ , right vertical axis, figure 3(b)] is about an order of magnitude less than  $\kappa$ . The experimentally observed sensitivity of the state selectivity to the interferometer phase suggests that this may be due to drifts of the interferometer's path-length difference during measurements, which we are only able to monitor to tens of nanometers. While the total number of detected photons per measurement is too low to allow single-shot measurement with this simple scheme, ensemble measurements allow clear state distinction, and coherent control techniques that are more sophisticated than this simple delay stage may be capable of allowing more cycling.

While the time-domain picture described above is sufficient for understanding the principles involved, the fact that we operate in the weak-pulse limit ( $\theta \ll \pi$ ) suggests the existence of a simple frequency-domain interpretation. In particular, it is tempting to view the Mach-Zehnder interferometer (figure 2(d)) as a *frequency filter* that allows the desired frequencies to pass while the rejected frequencies are sent to the unused output port. However, since the interferometer is implemented for the red (un-doubled) light, while the optical spectra exiting the two ports will be complimentary, they would produce almost indistinguishable spectra in the UV upon subsequent frequency doubling. This is because the difference between the intra-pulse-pair phases of the two ports in the red is  $\pi$ , which becomes  $2\pi$  after frequency doubling. The frequency domain description that is probably most apt, then, is that the red light interferometer controls the creation of the UV light so that power spectral density near undesired frequencies is not created in the first place. While this frequency domain interpretation is perfectly applicable for this work, this subtlety of the filtration is one reason we have chosen to instead focus primarily on the time-domain picture here, which will likely continue to be applicable for stronger pulses.

For electron-shelved and optical-frequency ion qubits, the temporal filtering enabled by the use of a mode-locked laser for state detection has allowed us to achieve a state preparation and measurement fidelity approaching the highest reported observation with this atom [4] and should be compatible with future integrated high efficiency, non-imaging detectors. Future development of ultrafast optical switches may someday allow extension of this idea to cw lasers [34]. For direct hyperfine qubit detection, the simple delay

scheme we have used here could be viewed as the minimal possible instance of coherent control, an approach that has been demonstrated in other contexts with far more sophisticated implementations. Nonetheless, this simple version has been sufficient to tease out and control the dynamics of a quantum 4-level system with  $\approx 30$  MHz precision and enable temporal filtering for qubit state detection. The fact that useful dynamical information can be extracted from a single atom with such a simple system is largely due to the high level of control that exists for the isolated quantum systems employed for quantum information processing, and it seems likely that further application of the approaches of coherent control to the pure state systems in quantum information science (particularly for many-qubit systems) will lead to new and potentially useful insights.

## Acknowledgments

The authors acknowledge Thomas Dellaert and Patrick McMillin for technical assistance, Adam West for graphical assistance, and E Hudson, P Hamilton, J Caram, and T Atallah for discussions. This work was supported by the U.S. Army Research Office under Grant No. W911NF-15-1-0261. CR and AR contributed equally to this work.

## References

- [1] DiVincenzo D P 2000 *Fortschr. Phys.* **48** 771
- [2] Gottesman D 2009 arXiv:0904.2557
- [3] Christensen J E, Hucul D, Campbell W C and Hudson E R 2019 arXiv:1907.13331
- [4] Noek R, Gaultney D, Mount E, Kim T, Maunz P, Kim J and Vrijsen G 2013 *Opt. Lett.* **38** 4735
- [5] Nagourney W, Sandberg J and Dehmelt H 1986 *Phys. Rev. Lett.* **56** 2797
- [6] Bergquist J C, Hulet R G, Itano W M and Wineland D J 1986 *Phys. Rev. Lett.* **57** 1699
- [7] Sauter T, Neuhauser W, Blatt R and Toschek P E 1986 *Phys. Rev. Lett.* **57** 1696
- [8] Acton M et al 2006 *Quantum Inf. Comput.* **6** 465
- [9] VanDevender A P, Colombe Y, Amini J, Leibfried D and Wineland D J 2010 *Phys. Rev. Lett.* **105** 023001
- [10] Merrill J T. 2011 *New J. Phys.* **13** 103005
- [11] Ghadimi M. 2017 *npj Quantum Inf.* **3** 4
- [12] Mehta K K, Eltony A M, Bruzewicz C D, Chuang I L, Ram R J, Sage J M and Chiaverini J 2014 *Appl. Phys. Lett.* **105** 044103
- [13] Guise N D 2015 *J. Appl. Phys.* **117** 174901
- [14] Maunz P L W et al 2015 *IARPA MQCO Technical Exchange*
- [15] Mehta K K, Bruzewicz C D, McConnell R, Ram R J, Sage J M and Chiaverini J 2016 *Nat. Nanotechnol.* **11** 1066
- [16] Kielpinski D, Volin C, Streed E W, Lenzini F and Lobino M 2016 *Quantum Inf. Process.* **15** 5315
- [17] Crain S, Cahall C, Vrijsen G, Wollman E E, Shaw M D, Verma V B, Nam S W and Kim J 2019 *Commun. Phys.* **2** 97
- [18] Eltony A M, Wang S X, Akselrod G M, Herskind P F and Chuang I L 2013 *Appl. Phys. Lett.* **102** 054106
- [19] Slichter D H, Verma V B, Leibfried D, Mirin R P, Nam S W and Wineland D J 2017 *Opt. Express* **25** 8705
- [20] Linke N, Allcock D, Szwed D, Ballance C, Harty T, Janacek H, Stacey D, Steane A and Lucas D 2011 *Appl. Phys. B: Lasers Opt.* **107** 1175–80
- [21] Hendricks R J, Sørensen J L, Champenois C, Knoop M and Drewsen M 2008 *Phys. Rev. A* **77** 021401
- [22] Dehmelt H G 1975 *Bull. Am. Phys. Soc.* **20** 60
- [23] Burt E and Nagourney W 1997 *Rev. Sci. Instrum.* **68** 1348
- [24] Yoshimura B, Stork M, Dacic D, Campbell W C and Freericks J K 2015 *EPJ Quantum Technol.* **2** 2
- [25] Olmschenk S, Younge K C, Moehring D L, Matsukevich D N, Maunz P and Monroe C 2007 *Phys. Rev. A* **76** 052314
- [26] Ransford A, Roman C, Dellaert T, McMillin P and Campbell W C 2020 in preparation
- [27] Olmschenk S, Hayes D, Matsukevich D N, Maunz P, Moehring D L, Younge K C and Monroe C 2009 *Phys. Rev. A* **80** 022502
- [28] Ip M, Ransford A, Jayich A M, Long X, Roman C and Campbell W C 2018 *Phys. Rev. Lett.* **121** 043201
- [29] Pruttivarasin T and Katori H 2015 *Rev. Sci. Instrum.* **86** 115106
- [30] Wollman E E 2017 *Opt. Express* **25** 26792
- [31] Loomis F W and Wood R W 1928 *Phys. Rev.* **32** 223
- [32] Kisiel Z, Pszczółkowski L, Medvedev I R, Winniewisser M, De Lucia F C and Herbst E 2005 *J. Mol. Spectrosc.* **233** 231
- [33] Lomsadze B and Cundiff S T 2017 *Science* **357** 1389
- [34] Koulakis J P and Putterman S 2019 *Opt. Lett.* **44** 3258